# Effects of noise on geophone orientation azimuth determination

Peter Gagliardi, Kristopher A. H. Innanen, and Don C. Lawton


## ABSTRACT

Calibration of the orientation of borehole geophones has direct consequences on the accuracy of subsequent measurements taken by these tools. Using synthetic data generated from a simple layer-cake geological model, the effects of signal to noise ratio, source-receiver offset and receiver depth were determined to have an effect on this calibration. A signal to noise ratio of 1 or better was generally found to produce mean orientation angles within 0.5° of the true value; however, even a noise-free signal produced small errors in the calibrations. It was also found that increasing offset and decreasing receiver depth both improve the accuracy of azimuth calculations. Effects of the three examined variables were judged to be difficult to separate from one another, although a quantitative relationship of these to azimuth calibration would be useful to develop.


## INTRODUCTION

Borehole geophones are a very important tool that geophysicists employ, having a distinct set of advantages over their surface counterparts. One of the more common uses of borehole geophones is in the field of microseismic monitoring; these receivers are used to estimate the position of subsurface seismic events. However, when placing these geophones into a well they have a tendency to rotate, resulting in an unknown orientation of their horizontal components. In order to determine the orientation of these borehole geophones, surface calibration surveys are generally performed; the accuracy of these calibrations will directly affect the accuracy of locating seismic events in the subsurface. The goal of this study will be to examine the combined effects of noise, receiver depth and source offset on the accuracy of a known geophone orientation. The main method that will be used to find geophone orientation is an analytic method developed by DiSiena et al. (1984); however, an inversion method developed by Ferguson (2009) will also be tested.

## SYNTHETIC MODEL

In order to generate the synthetic data for this report, a 3-D anisotropic elastic finite-difference program called TIGER was used (Hokstad et al., 2009). A simple 6 layer geological model was built; acquisition parameters can be seen in Table 1, model parameters can be seen numerically in Table 2, and a visual representation can be seen in Figure 1. While specification of anisotropic parameters and Q values are supported by TIGER (Hokstad et al., 2009), they were omitted for the purposes of this study. Additionally, a plan view of the survey geometry is shown in Figure 2. All receivers recorded 3-component data; due to limitations of the program, receiver components were all forced to be aligned perfectly with model coordinates. Finally, raw x-component data from Shot 1 can be seen in Figure 3.

Table 1. Numerical parameters used for acquisition in this study.

| TIGER Acquisition Parameters | |
|---|---|
| Maximum x | 3000 m |
| Maximum y | 3000 m |
| Maximum z | 2500 m |
| x interval | 10 m |
| y interval | 10 m |
| z interval | 10 m |
| Recording time | 1400 ms |
| Source type | Zero-phase |
| Number of sources | 20 |
| Source interval | 149 m |
| Number of receivers | 64 |
| Receiver interval | 15 m |

Table 2. Numerical parameters used to create the geological model used in this study.

| Layer | Depth to top (m) | Density (kg/m$^3$) | P-velocity (m/s) | S-velocity (m/s) |
|---|---|---|---|---|
| 1 | 0 | 1000 | 1480 | 0 |
| 2 | 250 | 2000 | 2000 | 1200 |
| 3 | 650 | 1500 | 2500 | 1500 |
| 4 | 950 | 2500 | 3000 | 2000 |
| 5 | 1450 | 2600 | 3200 | 2100 |
| 6 | 2000 | 2600 | 3500 | 2200 |

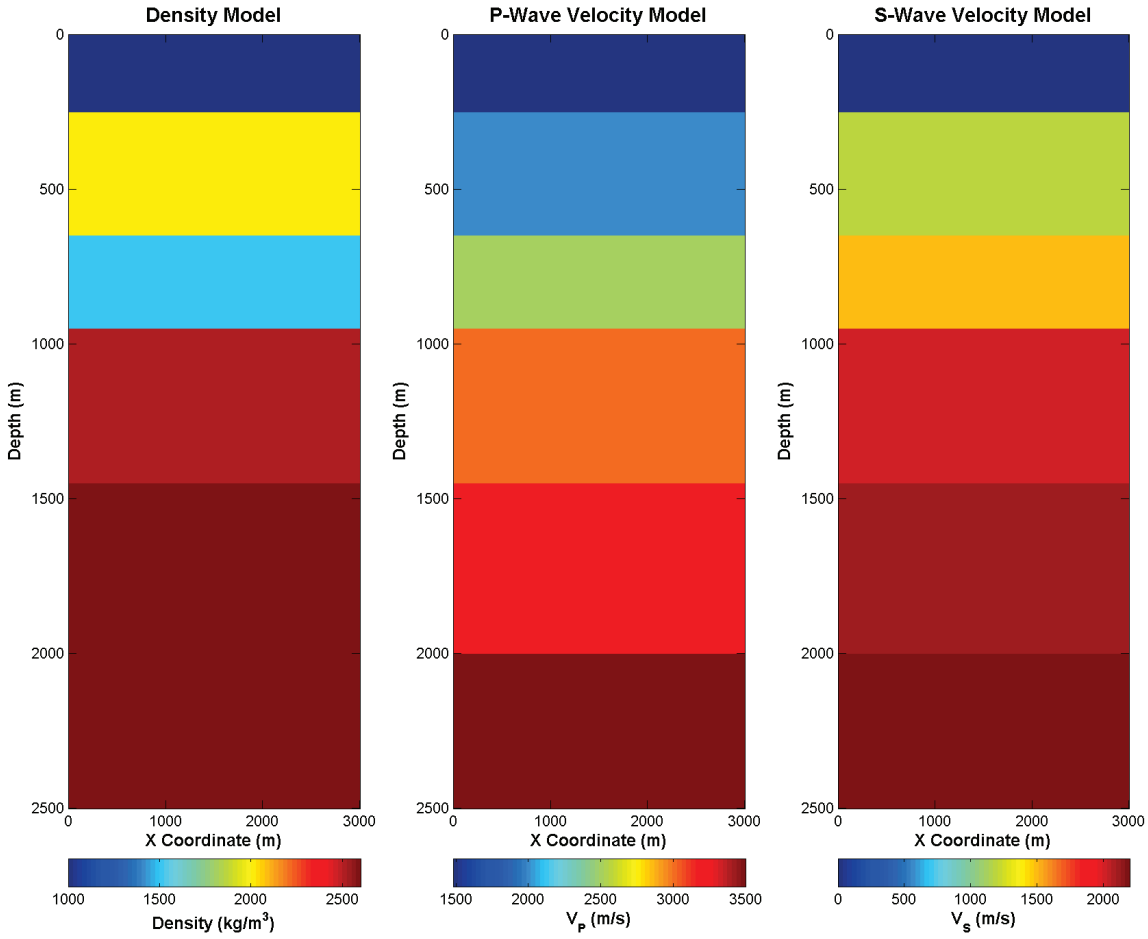


FIG. 1. 2-D slice of the geological model used in this study. Density is shown on the left, P-velocity is shown in the middle, and S-velocity is shown on the right.

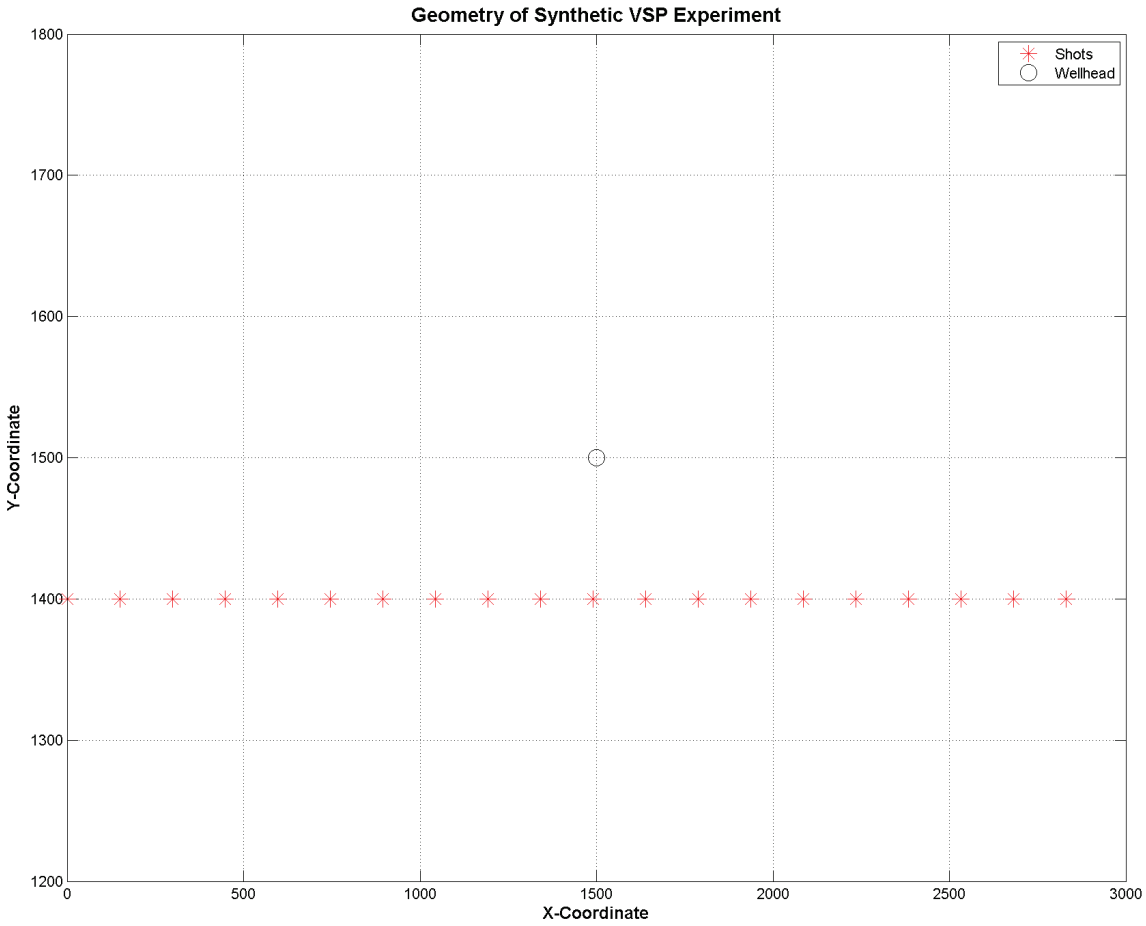


FIG. 2. Plan view of acquisition geometry used in this experiment.

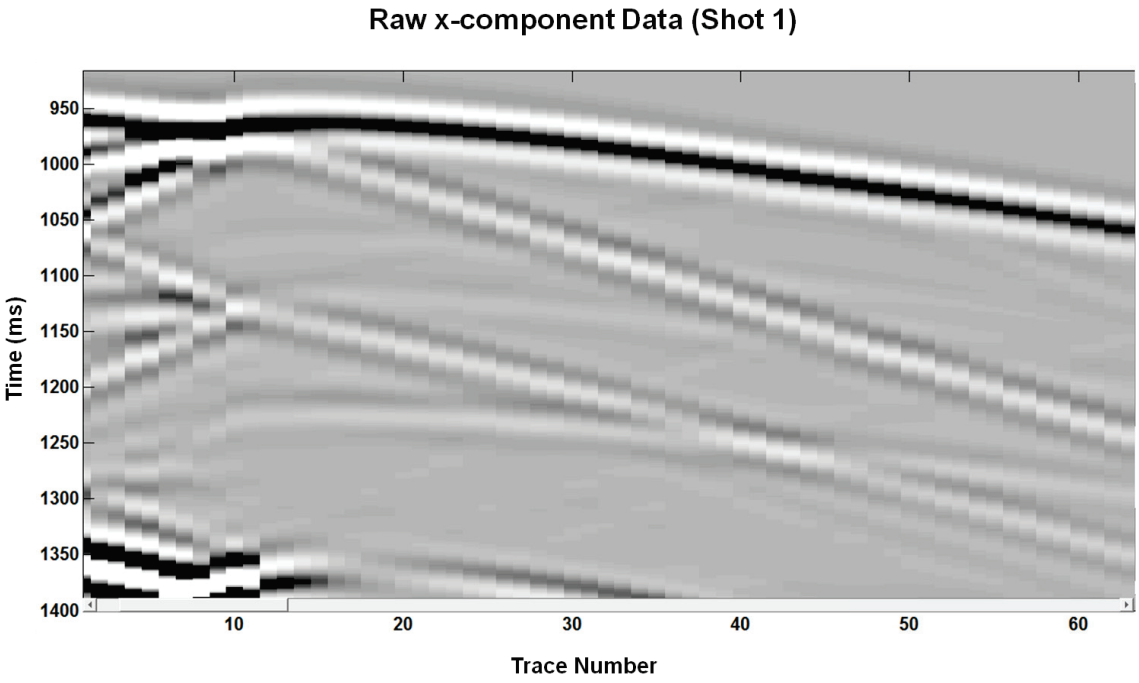


FIG. 3. Raw x-component data from Shot 1, prior to addition of noise.

## ADDITIVE NOISE

### Noise Generation

The noise used in this study was generated using the *rnoise* command in MATLAB, using trace 513 of the y-component as a reference. Signal to noise ratios used were 0.05, 0.1, 0.2, 0.5, 1, 2, 5, 10, and 20; noise was generated separately for each receiver component (Figure 4). It would be interesting to examine different noise relationships between components; for example, adding noise to the y-component that is identical to the noise on the x-component, but phase shifted by 90°. However, this is beyond the scope of this study and will have to be left as a future exercise. Finally, in order to examine the effects of coherent noise, 60 Hz sine waves were generated with signal to noise ratios of 0.5, 1, 2 and 10.

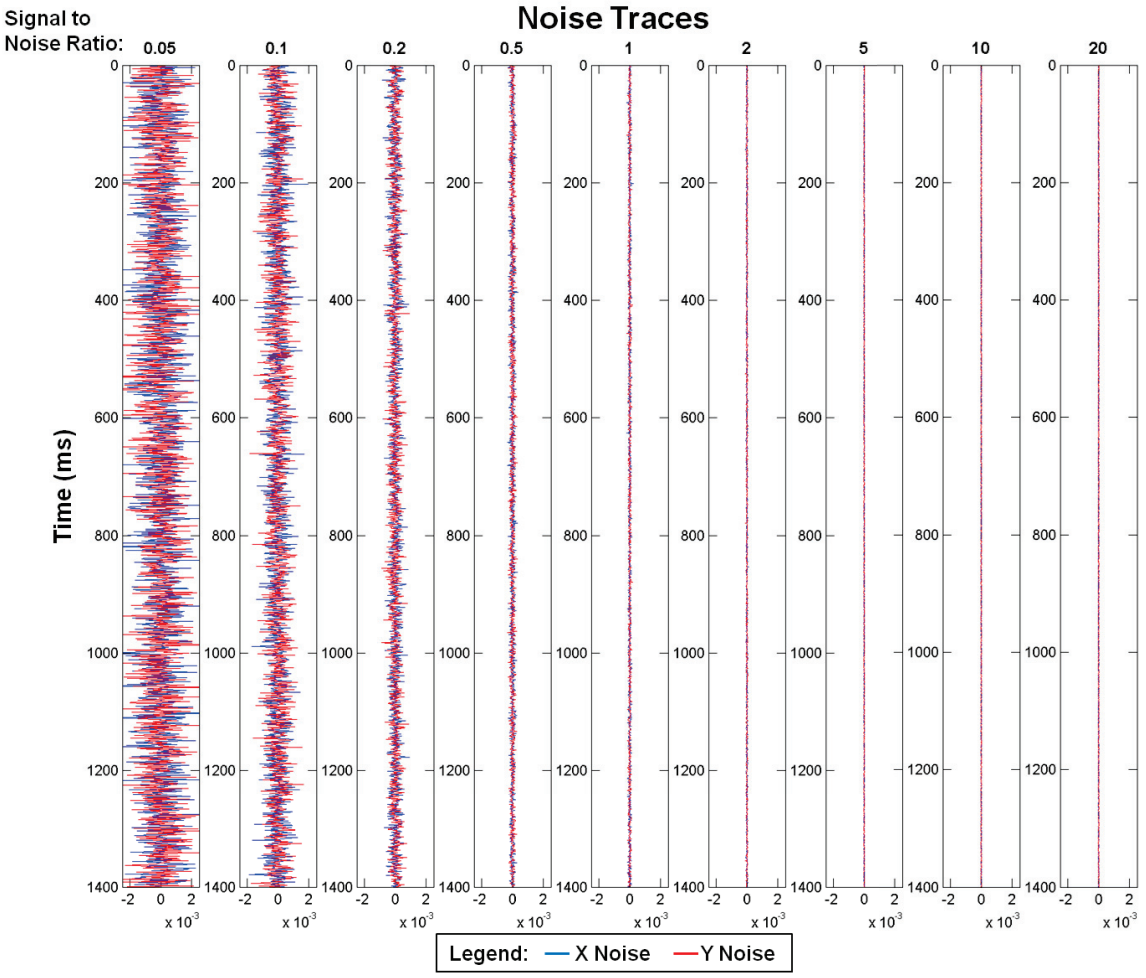


FIG. 4. Noise added to synthetic data; noise added to the x-component is shown in blue, and noise added to the y-component is shown in red. Signal to noise ratio is given at the top of each trace.

### Noise Addition

After generating the noise, it was added to the synthetic traces in two specific patterns. In Noise Pattern 1, receivers 1-59 were separated into groups of 10; each receiver was

assigned a different signal to noise ratio, in order from noisiest to cleanest, with the 10th receiver in each group being left clean. The next 4 receivers, 60-63, had the different sine waves added to each component, again in order from noisiest to cleanest. Finally geophone 64 sine waves of differing power added to each component; the signal to noise ratio on the x-component was 10, that on the y-component was 1, and that on the z-component was 2. This pattern was repeated for all 20 shots; as an example, Shot 1 is shown after the addition of noise in Figure 5.

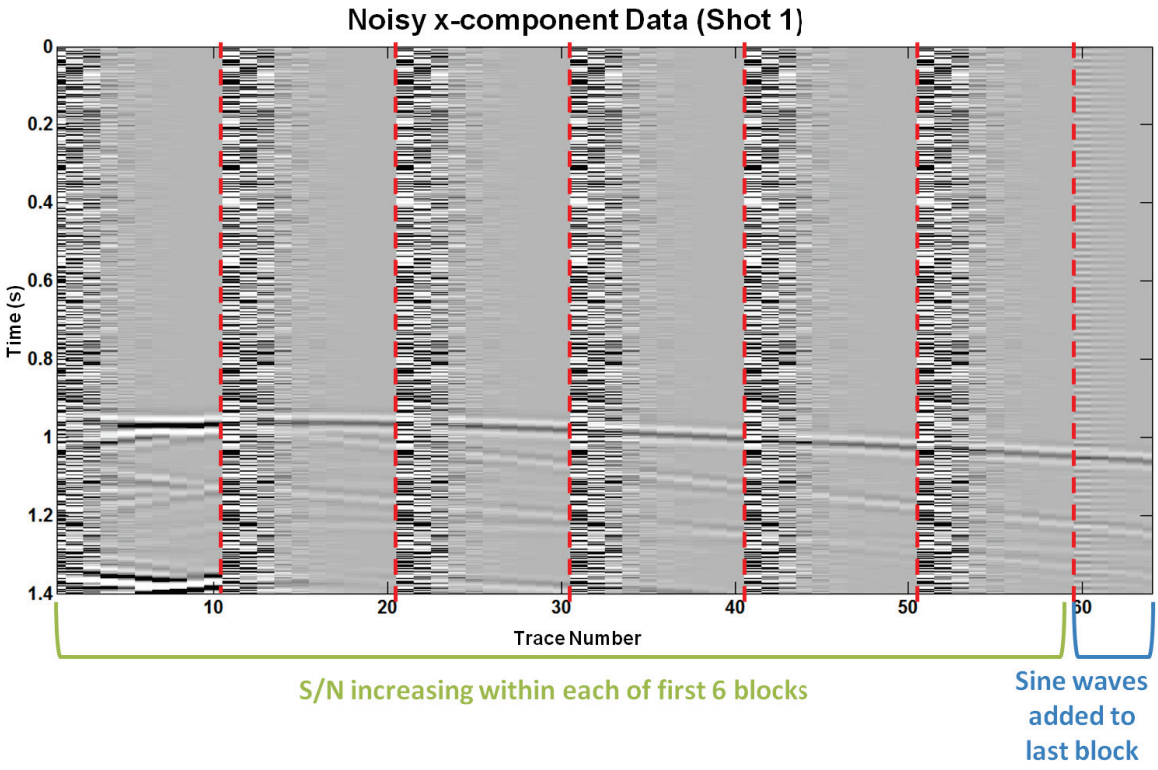


FIG. 5. X-component data from Shot 1, after the addition of noise.

For Noise Pattern 2, 8 receivers were selected; these were at depths of 800 m, 920 m, 1040 m, 1160 m, 1280 m, 1400 m, 1520 m and 1640 m. For each of these receivers, all 9 different noisy traces were added, leaving a total 1440 traces to examine. Once noise was added, geophone orientation analysis was performed on the data.

## ROTATION METHODS

A simple analytic method for determining geophone orientation can be given by (DiSiena et al., 1984)

$$\tan 2\theta = \frac{2X \otimes Y}{X \otimes X + Y \otimes Y}, \tag{1}$$

where X and Y are the horizontal component data, $\theta$ is the angle between the x-component and the source, and $\otimes$ is a crosscorrelation operator. Additionally, an inversion method developed by Ferguson (2009) will be tested. This method views the

mapping of recorded multicomponent data (V) into a single trace aligned with the incoming P-wave (W), through a single rotation matrix $G_{\theta\phi}$, expressed as

$$W = G_{\theta\phi}V = \begin{bmatrix} \cos\theta & \sin\theta\cos\phi & \sin\theta\sin\phi \\ -\sin\theta & \cos\theta\cos\phi & \cos\theta\sin\phi \\ 0 & -\sin\phi & \cos\phi \end{bmatrix} V, \quad (2)$$

where $\phi$ is the angle between the z-component and the incoming P-wave (Ferguson, 2009). The inverse of $G_{\theta\phi}$ is found through least squares inversion, under the assumption that all time samples of the recorded z-component data are the same sign as the ideal P-wave source, within a specified window. The values for $\theta$ and $\phi$ can subsequently be extracted from the calculated inverse. A 100 ms window beginning at the first break was used for both the analytic method and the inversion.

Once $\theta$ is found, it can be converted into an azimuth relative to North using

$$\phi_r = \phi_s + \theta, \quad (3)$$

where $\phi_s$ is the source-receiver azimuth, relative to North, and $\phi_r$ is the receiver orientation azimuth. Conversion to the receiver orientation azimuth provides a standard reference frame for all potential source locations. Since the receiver components are aligned perfectly with the model coordinates, all receivers have an orientation azimuth of 90°.

## RESULTS

### Analytic (DiSiena) Method

*Noise Pattern 1*

Once the receiver orientation azimuth was found for every receiver, the results were plotted against source-receiver horizontal offset; values calculated from the noise-free synthetic data are also shown for comparison (Figures 6 - 8). Additionally, Figures 9 - 11 show receivers with similar noise content. There is a clear relationship between noise and angle scatter; once the signal to noise ratio reaches approximately 1, the angle seems to be much better constrained. Quantitative analysis (Table 3) reveals that the standard deviation at a signal to noise ratio of 1 ranges from 1.24°-7.69°, whereas a signal to noise ratio of 0.5 produces standard deviations as high as 22.2°. Furthermore, Table 3 and Figure 12 demonstrate that increasing receiver depth is well correlated with higher angle scatter; this is to be expected, as a deeper geophone will receive a weaker signal from the source.

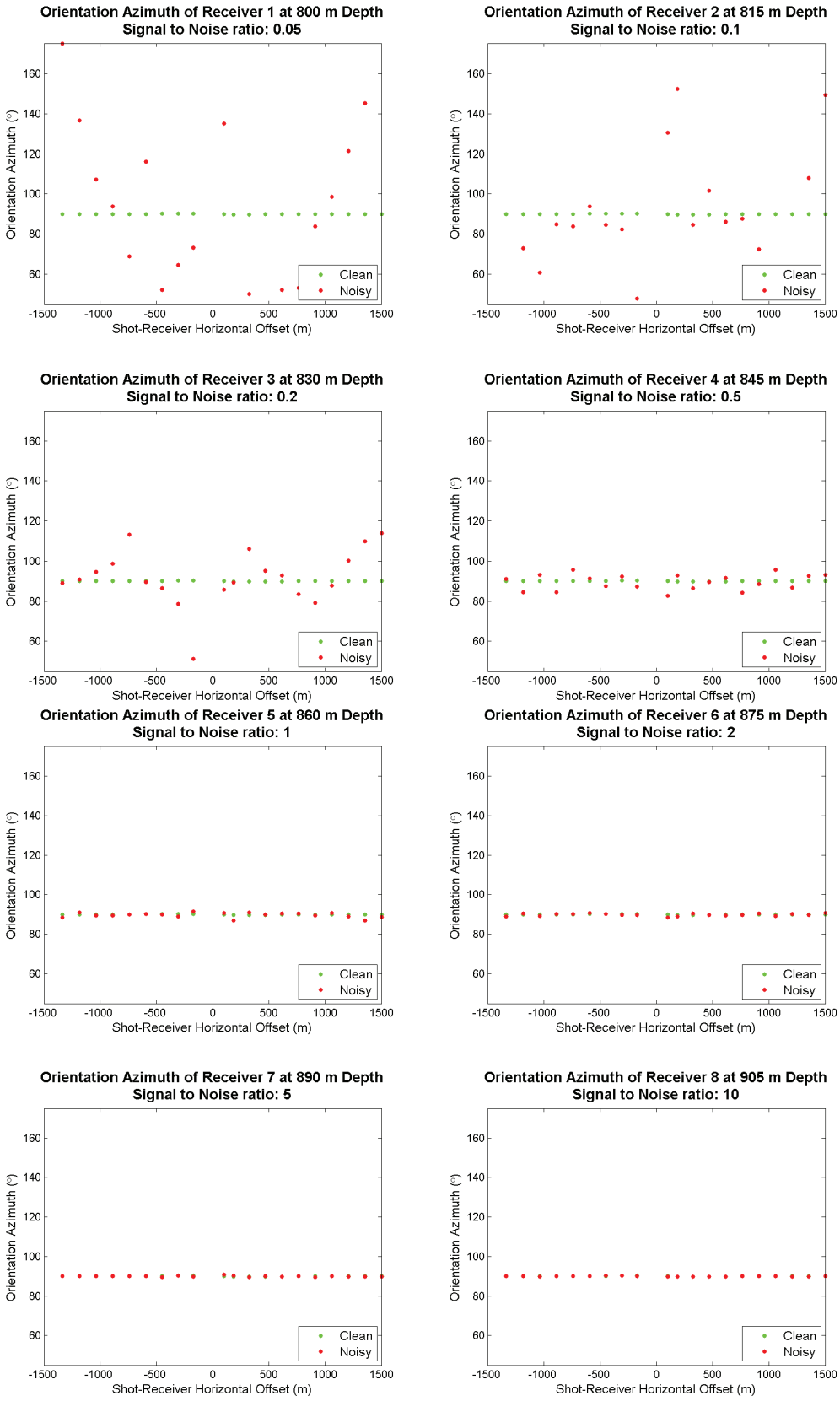


FIG. 6. Orientation azimuth vs. horizontal offset for receivers 1-8. Noisy data is shown in red, noise-free data is shown in green.

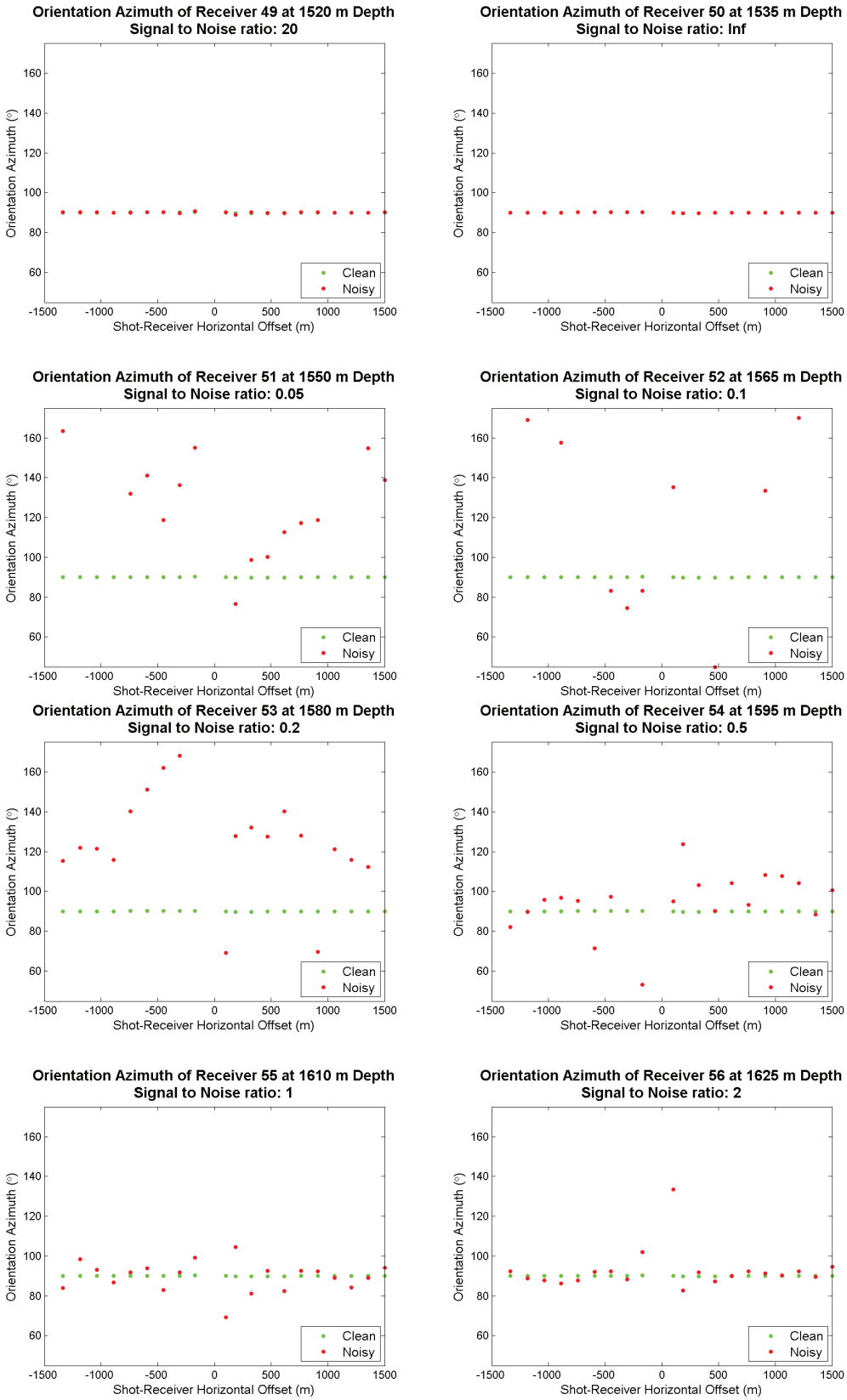


FIG. 7. Orientation azimuth vs. horizontal offset for receivers 49-56. Noisy data is shown in red, noise-free data is shown in green.

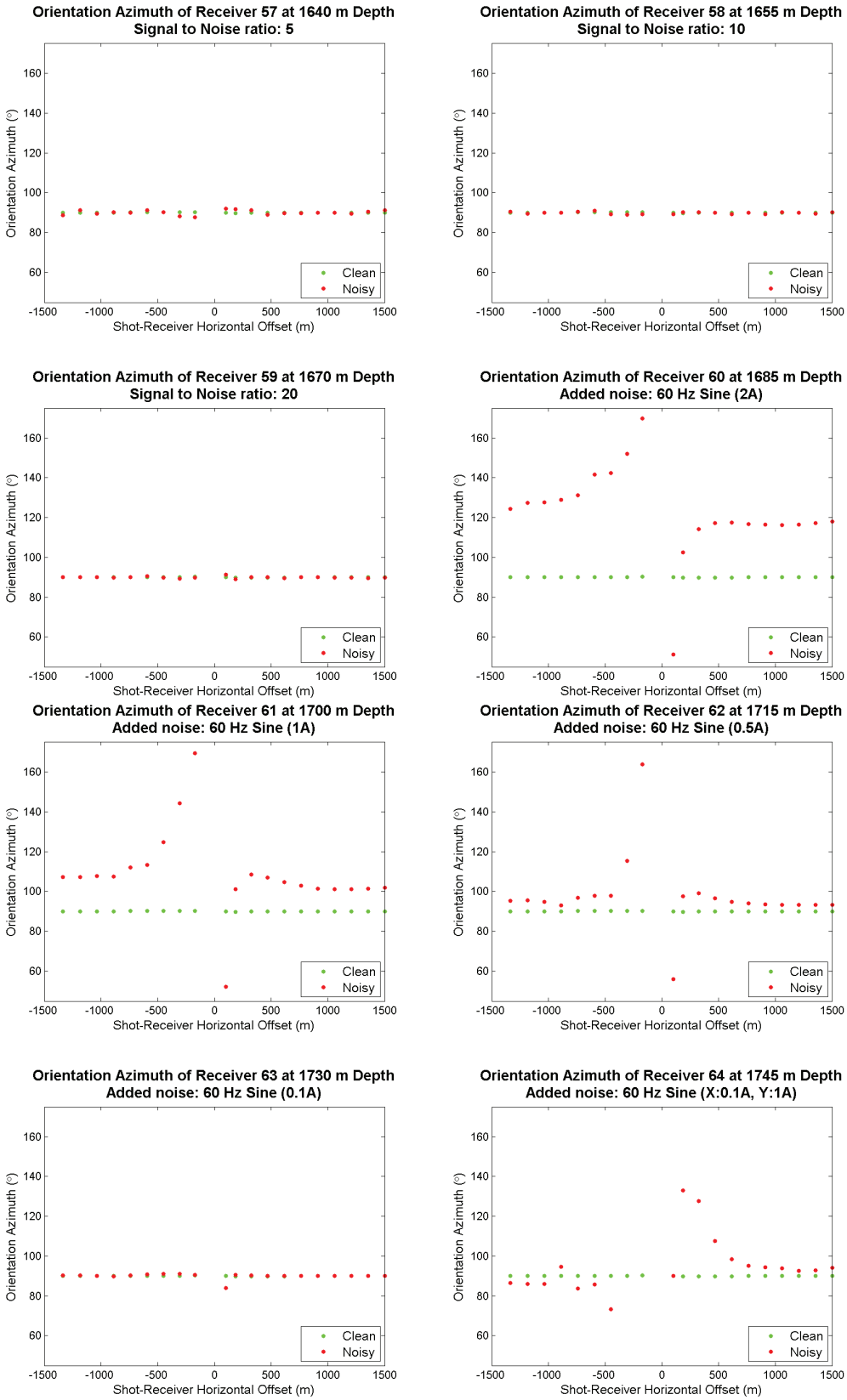


FIG. 8. Orientation azimuth vs. horizontal offset for receivers 57-64. Noisy data is shown in red, noise-free data is shown in green.

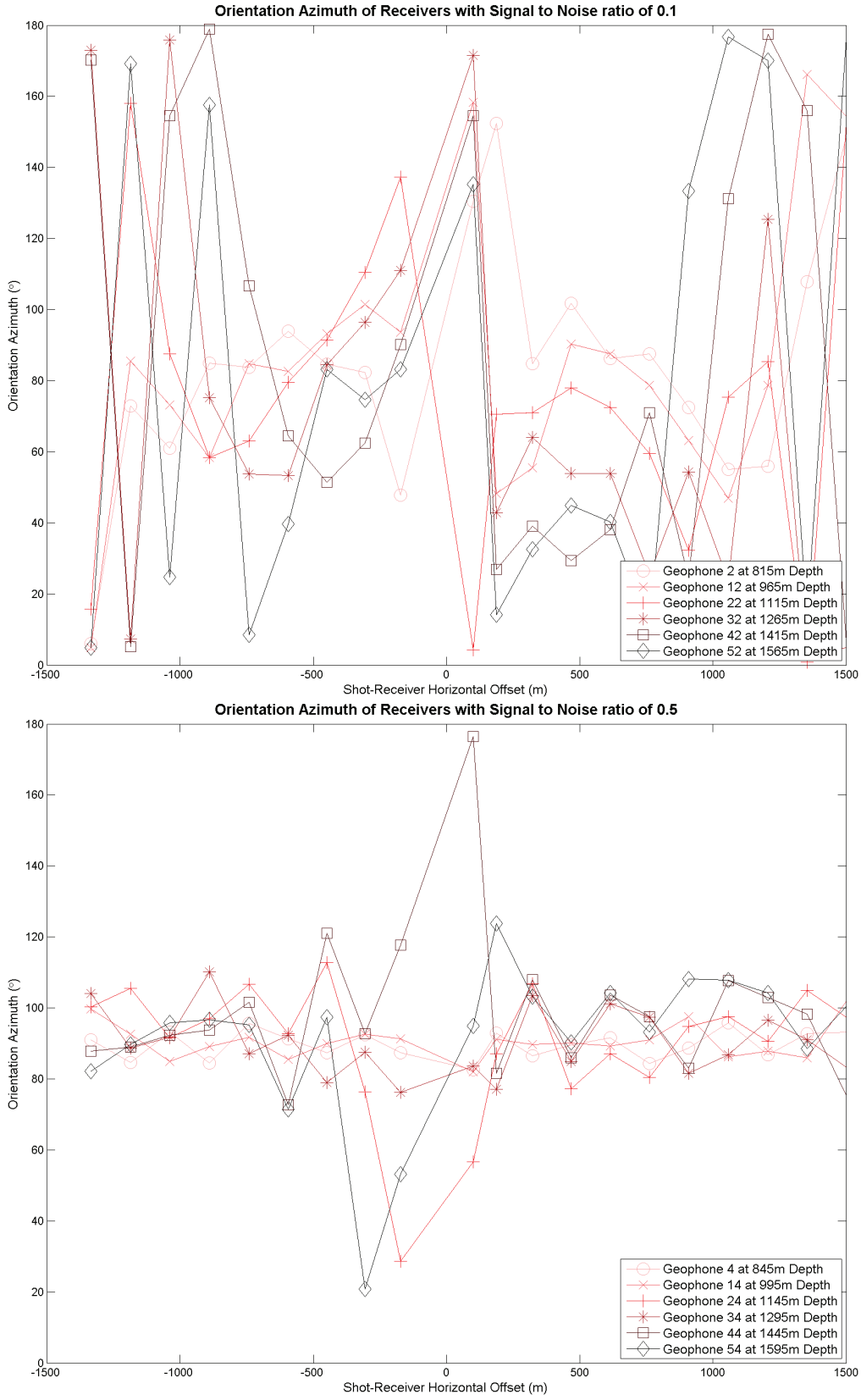


FIG. 9. Orientation azimuth vs. horizontal offset for receivers with signal to noise ratios of 0.1 (top) and 0.5 (bottom), calculated analytically. Darker colours correspond to larger depths.

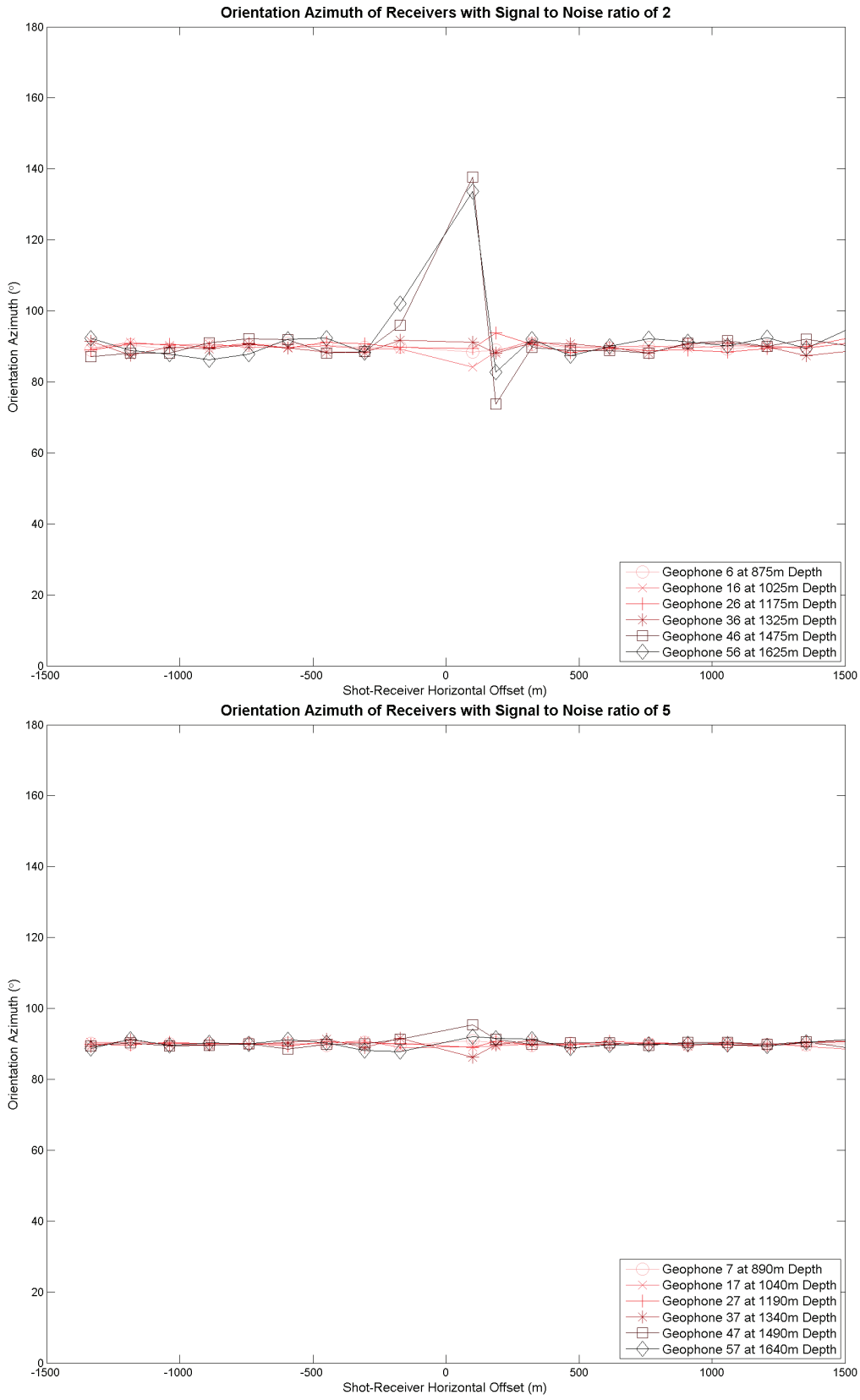


FIG. 10. Orientation azimuth vs. horizontal offset for receivers with signal to noise ratios of 2 (top) and 5 (bottom), calculated analytically. Darker colours correspond to larger depths.

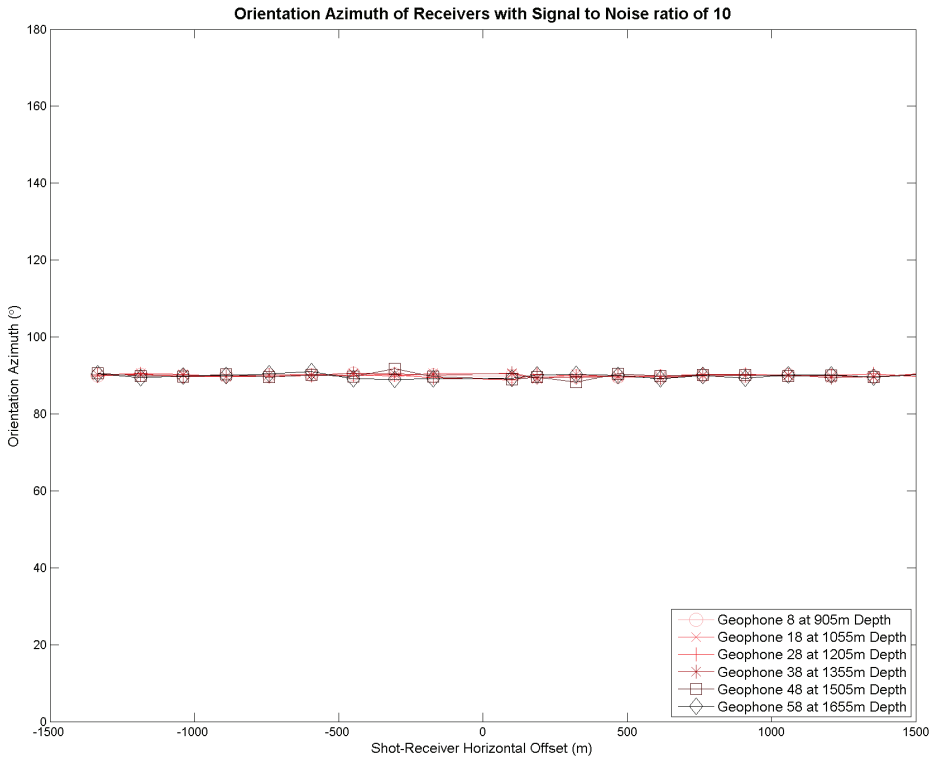


FIG. 11. Orientation azimuth vs. horizontal offset for receivers with a signal to noise ratio of 10, calculated analytically. Darker colours correspond to larger depths.

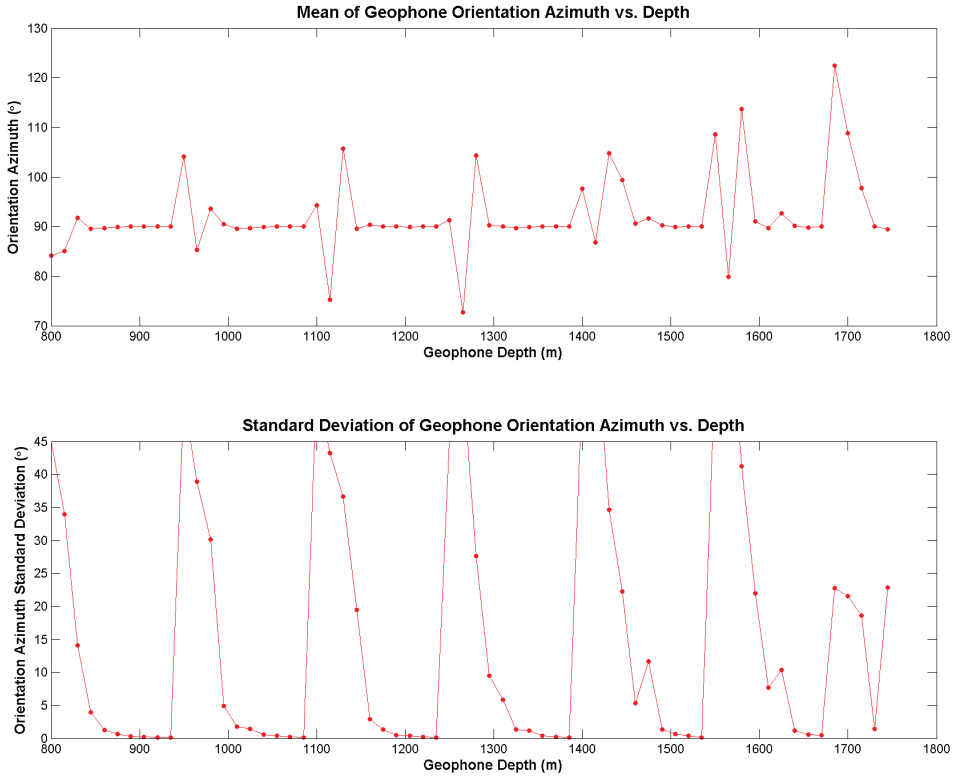


FIG. 12. Mean geophone orientation azimuth (top) and standard deviation (bottom) vs. receiver depth.

Table 3. Geophone orientation statistics of angles calculated analytically using Noise Pattern 1.

| | | | | | | | |
|---|---|---|---|---|---|---|---|
| **Signal to Noise: 0.05** | Depth (m) | 800 | 950 | 1100 | 1250 | 1400 | 1550 |
| | Mean (°) | 84.14 | 104.14 | 94.25 | 91.34 | 97.68 | 108.63 |
| | St. Dev (°) | 45.09 | 50.80 | 52.84 | 46.57 | 55.75 | 55.23 |
| **Signal to Noise: 0.1** | Depth (m) | 815 | 965 | 1115 | 1265 | 1415 | 1565 |
| | Mean (°) | 85.04 | 85.27 | 75.29 | 72.66 | 86.81 | 79.83 |
| | St. Dev (°) | 33.92 | 38.87 | 43.20 | 54.53 | 61.37 | 65.36 |
| **Signal to Noise: 0.2** | Depth (m) | 830 | 980 | 1130 | 1280 | 1430 | 1580 |
| | Mean (°) | 91.78 | 93.62 | 105.72 | 104.29 | 104.81 | 113.63 |
| | St. Dev (°) | 14.06 | 30.12 | 36.60 | 27.62 | 34.66 | 41.19 |
| **Signal to Noise: 0.5** | Depth (m) | 845 | 995 | 1145 | 1295 | 1445 | 1595 |
| | Mean (°) | 89.59 | 90.54 | 89.60 | 90.20 | 99.42 | 91.07 |
| | St. Dev (°) | 3.94 | 4.93 | 19.43 | 9.47 | 22.20 | 22.00 |
| **Signal to Noise: 1** | Depth (m) | 860 | 1010 | 1160 | 1310 | 1460 | 1610 |
| | Mean (°) | 89.67 | 89.55 | 90.34 | 89.99 | 90.59 | 89.67 |
| | St. Dev (°) | 1.24 | 1.75 | 2.88 | 5.82 | 5.35 | 7.69 |
| **Signal to Noise: 2** | Depth (m) | 875 | 1025 | 1175 | 1325 | 1475 | 1625 |
| | Mean (°) | 89.85 | 89.70 | 90.07 | 89.65 | 91.65 | 92.68 |
| | St. Dev (°) | 0.66 | 1.47 | 1.32 | 1.37 | 11.63 | 10.36 |
| **Signal to Noise: 5** | Depth (m) | 890 | 1040 | 1190 | 1340 | 1490 | 1640 |
| | Mean (°) | 90.02 | 89.88 | 90.04 | 89.89 | 90.28 | 90.09 |
| | St. Dev (°) | 0.31 | 0.56 | 0.50 | 1.17 | 1.37 | 1.15 |
| **Signal to Noise: 10** | Depth (m) | 905 | 1055 | 1205 | 1355 | 1505 | 1655 |
| | Mean (°) | 89.97 | 90.03 | 89.93 | 89.99 | 89.91 | 89.84 |
| | St. Dev (°) | 0.20 | 0.39 | 0.36 | 0.39 | 0.68 | 0.55 |
| **Signal to Noise: 20** | Depth (m) | 920 | 1070 | 1220 | 1370 | 1520 | 1670 |
| | Mean (°) | 90.00 | 90.02 | 90.00 | 90.06 | 90.04 | 89.97 |
| | St. Dev (°) | 0.13 | 0.18 | 0.20 | 0.18 | 0.35 | 0.45 |
| **Signal to Noise: Infinity** | Depth (m) | 935 | 1085 | 1235 | 1385 | 1535 | --- |
| | Mean (°) | 90.01 | 90.01 | 90.01 | 90.01 | 90.01 | --- |
| | St. Dev (°) | 0.12 | 0.11 | 0.12 | 0.11 | 0.11 | --- |

*Noise Pattern 2*

Noise Pattern 2 allowed for a more distinct separation between effects of noise and geophone depth. Figures 13 and 14 show how receiver depth affects the mean and standard deviation of calculated orientation azimuth, and Figures 15 and 16 show how noise affects these two parameters. The analysis of Noise Pattern 2 confirms what was seen in Noise Pattern 1, though perhaps more definable trends are evident. For example, Figure 16 shows an almost hyperbolic relationship between the natural logs of standard deviation and signal to noise ratio; however, the methods used to generate the noise most likely have an impact on this relationship. Table 4 summarizes the statistics of this analysis; generally, angle scatter appears to increase dramatically when the signal to noise ratio is less than 1, which is consistent with the results from Noise Pattern 1.

Table 4. Geophone orientation statistics of angles calculated analytically using Noise Pattern 2.

| | Depth (m) | 800 | 920 | 1040 | 1160 | 1280 | 1400 | 1520 | 1640 |
|---|---|---|---|---|---|---|---|---|---|
| **Signal to Noise: 0.05** | Mean (°) | 92.27 | 81.17 | 89.48 | 102.56 | 92.92 | 95.52 | 94.90 | 111.50 |
| | St. Dev (°) | 46.93 | 47.42 | 47.28 | 47.14 | 52.33 | 53.37 | 58.57 | 58.19 |
| **Signal to Noise: 0.1** | Mean (°) | 78.42 | 82.59 | 103.22 | 71.14 | 89.89 | 72.75 | 73.40 | 98.47 |
| | St. Dev (°) | 40.47 | 32.20 | 45.79 | 49.28 | 56.45 | 64.02 | 61.68 | 72.77 |
| **Signal to Noise: 0.2** | Mean (°) | 96.16 | 93.53 | 105.65 | 108.73 | 103.55 | 114.67 | 107.70 | 94.13 |
| | St. Dev (°) | 12.16 | 14.57 | 24.86 | 35.01 | 32.72 | 35.03 | 49.00 | 45.27 |
| **Signal to Noise: 0.5** | Mean (°) | 90.07 | 91.72 | 89.19 | 90.22 | 91.77 | 100.36 | 80.93 | 101.62 |
| | St. Dev (°) | 4.14 | 4.37 | 14.55 | 21.98 | 15.35 | 21.17 | 32.12 | 35.47 |
| **Signal to Noise: 1** | Mean (°) | 90.20 | 90.23 | 90.43 | 89.17 | 89.48 | 87.14 | 87.31 | 90.21 |
| | St. Dev (°) | 1.05 | 1.68 | 1.65 | 4.69 | 7.45 | 9.98 | 9.11 | 19.71 |
| | Depth (m) | 800 | 920 | 1040 | 1160 | 1280 | 1400 | 1520 | 1640 |
| **Signal to Noise: 2** | Mean (°) | 90.14 | 90.04 | 89.79 | 89.24 | 88.66 | 89.85 | 89.80 | 91.63 |
| | St. Dev (°) | 0.71 | 0.74 | 1.67 | 3.18 | 3.39 | 2.20 | 7.36 | 12.44 |
| **Signal to Noise: 5** | Mean (°) | 90.03 | 89.95 | 89.88 | 89.80 | 90.12 | 90.26 | 90.11 | 89.45 |
| | St. Dev (°) | 0.29 | 0.38 | 0.74 | 1.02 | 0.85 | 0.83 | 2.16 | 1.43 |
| **Signal to Noise: 10** | Mean (°) | 90.01 | 89.94 | 90.09 | 90.01 | 89.96 | 90.03 | 89.89 | 90.17 |
| | St. Dev (°) | 0.26 | 0.21 | 0.57 | 0.38 | 0.38 | 0.60 | 1.09 | 1.80 |
| **Signal to Noise: 20** | Mean (°) | 90.00 | 90.00 | 89.99 | 90.02 | 90.02 | 89.96 | 89.95 | 90.14 |
| | St. Dev (°) | 0.14 | 0.15 | 0.18 | 0.19 | 0.23 | 0.41 | 0.46 | 0.92 |

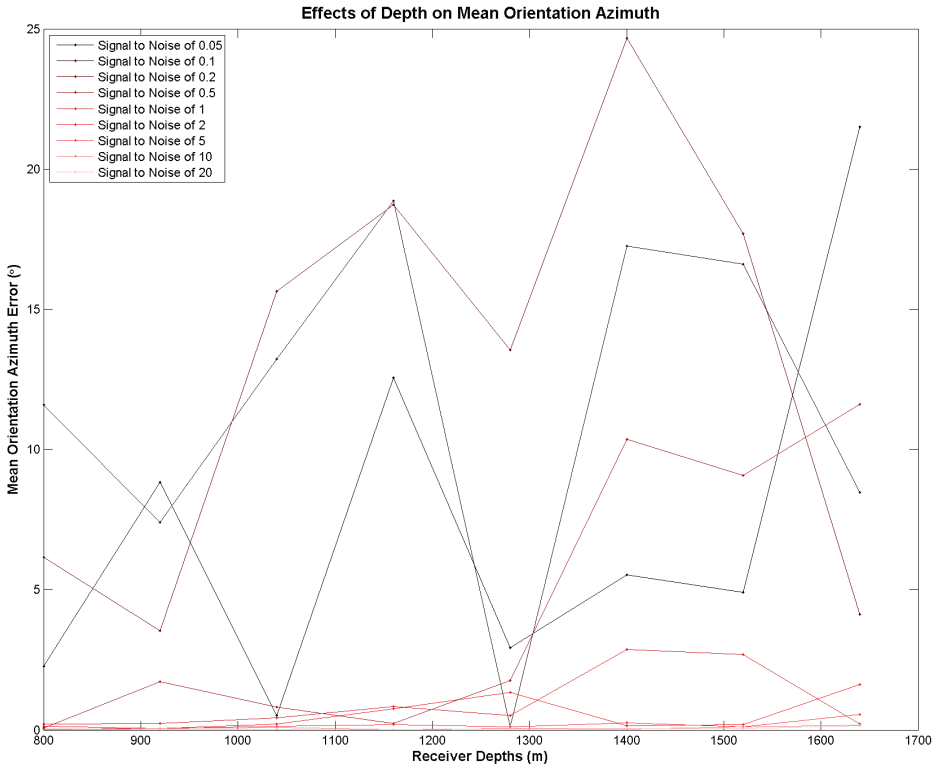


FIG. 13. Mean orientation azimuth error vs. receiver depth for Noise Pattern 2. Darker colours correspond to lower signal to noise ratios.

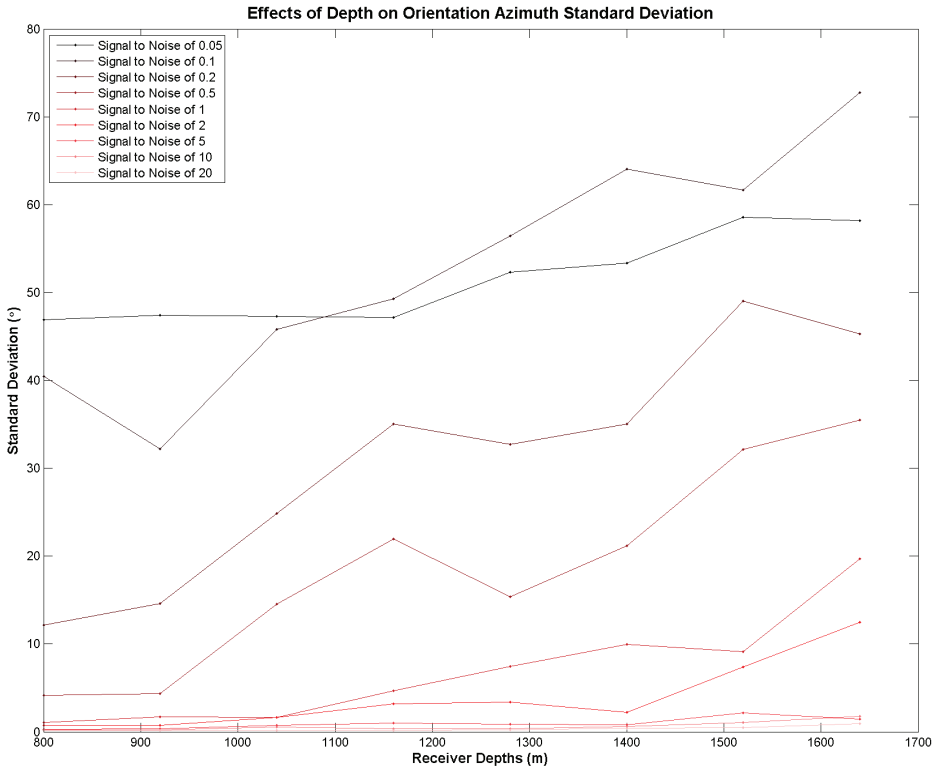


FIG. 14. Standard deviation of orientation azimuth vs. receiver depth for Noise Pattern 2. Darker colours correspond to lower signal to noise ratios.

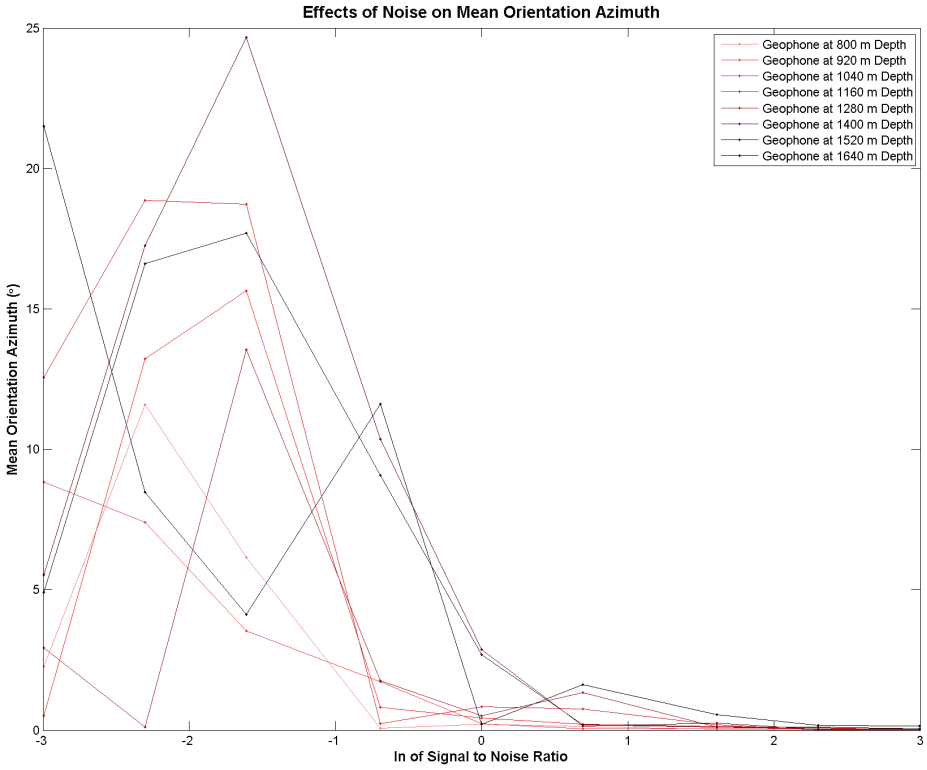


FIG. 15. Error in mean orientation azimuth vs. natural log of signal to noise ratio for Noise Pattern 2. Darker colours correspond to larger depths.

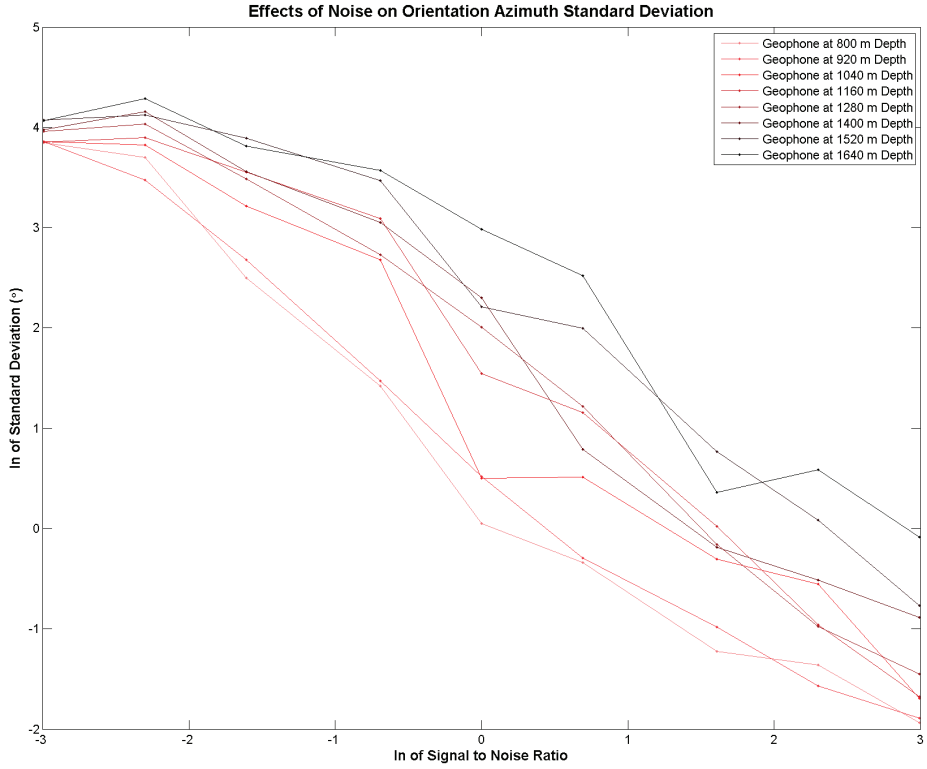


FIG. 16. Natural log of standard deviation of orientation azimuth vs. natural log of signal to noise ratio for Noise Pattern 2. Darker colours correspond to larger depths.

## Inversion (Ferguson) Method

The inversion method was tested on Noise Pattern 1, allowing a qualitative comparison to the analytic method; a full comparison, however, is beyond the scope of this study. Figures 17 - 20 can be directly compared to Figures 9 - 11; the inversion method appears to work much better in noisy situations, while the analytic method becomes more constrained once the signal to noise ratio reaches 1.

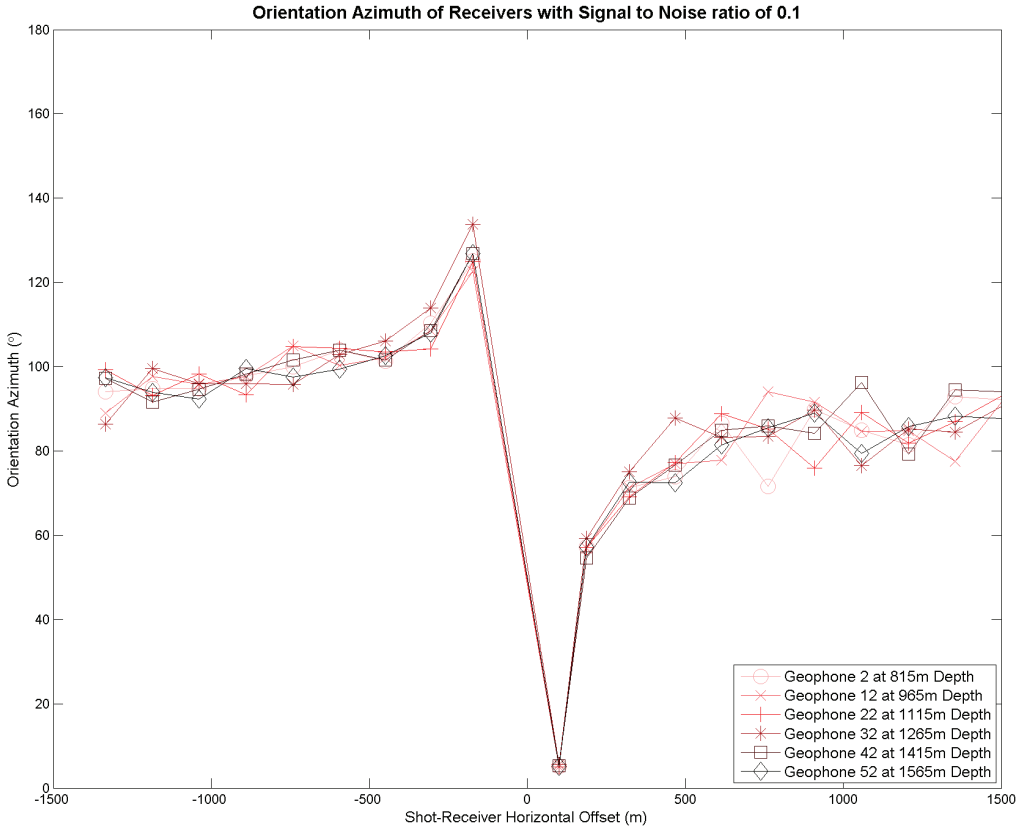


FIG. 17. Orientation azimuth vs. horizontal offset for receivers with a signal to noise ratio of 0.1, calculated using inversion method. Darker colours correspond to larger depths.

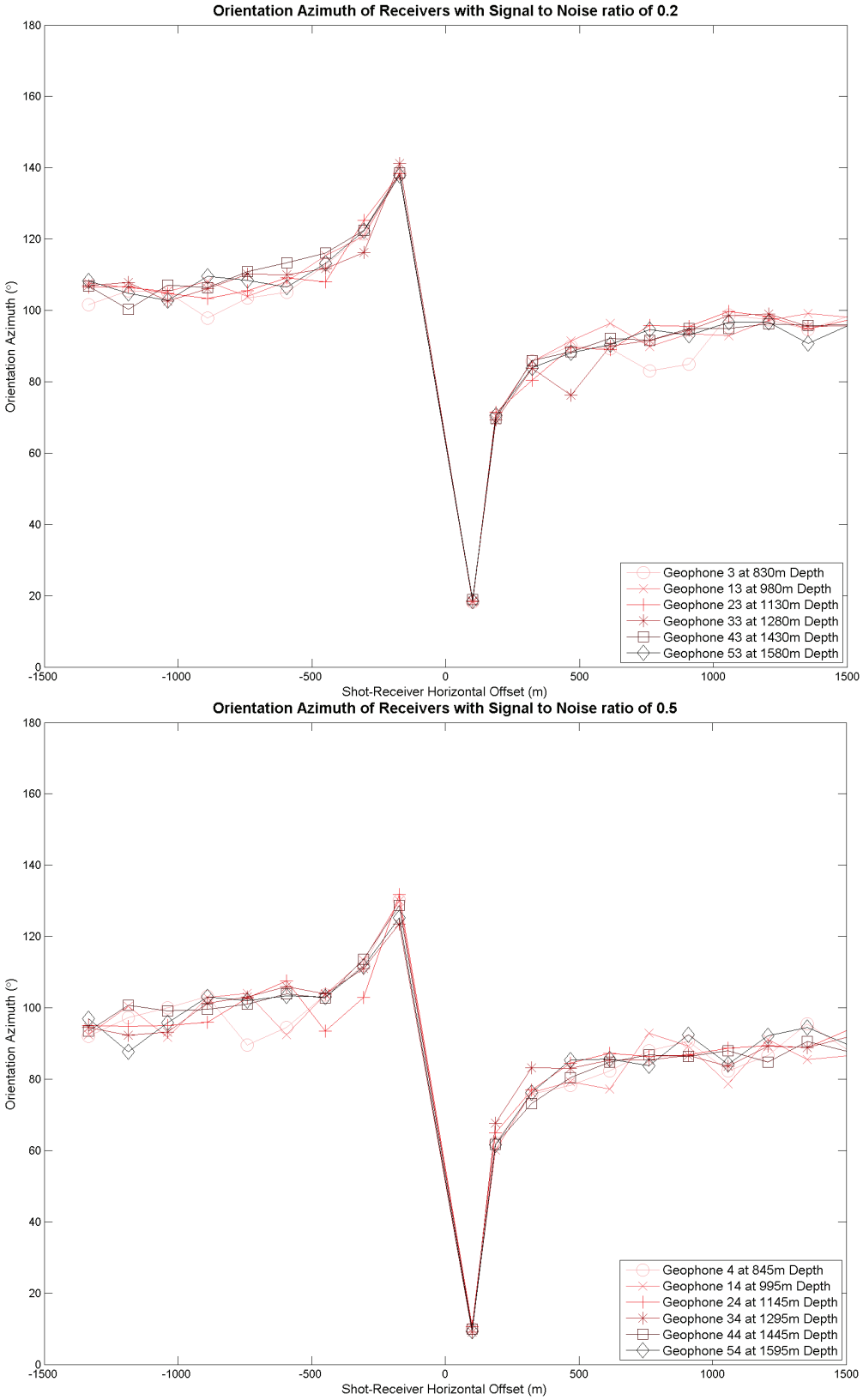


FIG. 18. Orientation azimuth vs. horizontal offset for receivers with signal to noise ratios of 0.1 (top) and 0.5 (bottom), calculated using inversion method. Darker colours correspond to larger depths.

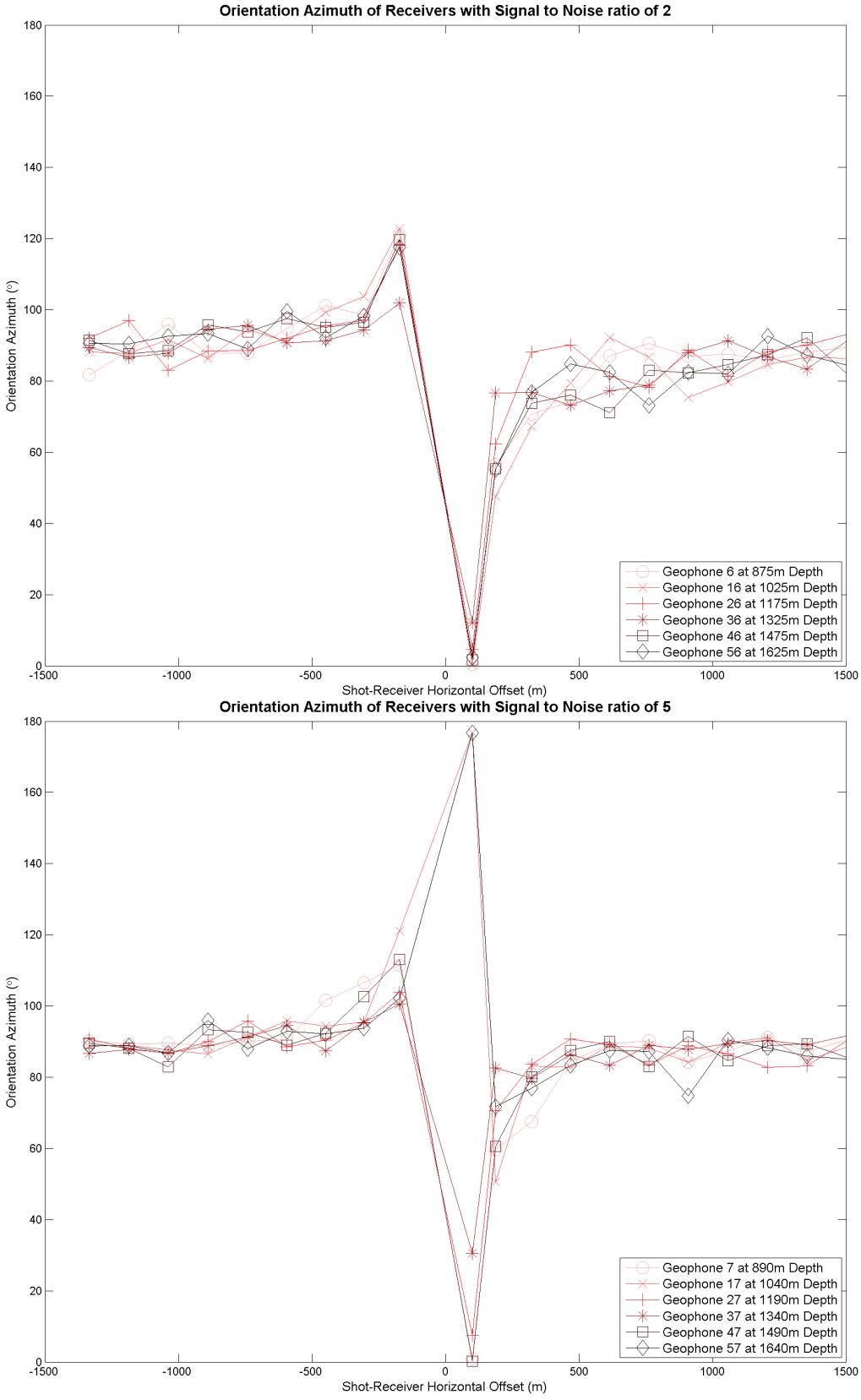


FIG. 19. Orientation azimuth vs. horizontal offset for receivers with signal to noise ratios of 2 (top) and 5 (bottom), calculated using inversion method. Darker colours correspond to larger depths.

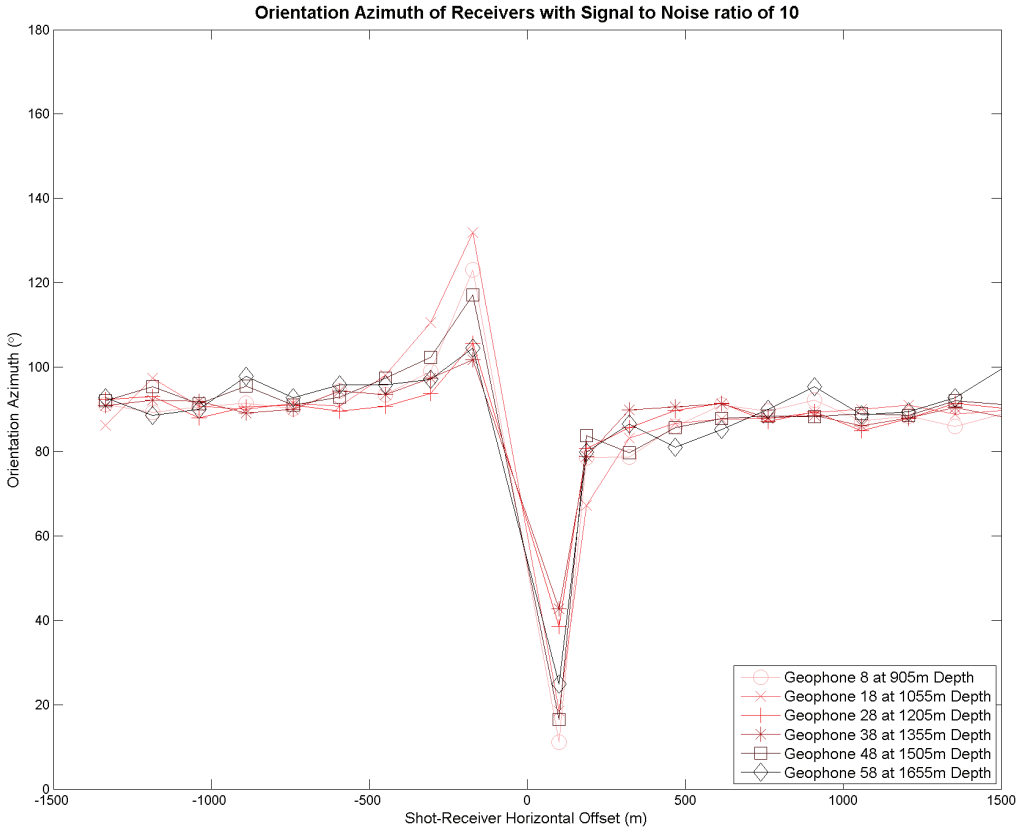


FIG. 20. Orientation azimuth vs. horizontal offset for receivers with a signal to noise ratio of 10, calculated using inversion method. Darker colours correspond to larger depths.

## DISCUSSION

The results of this study show a definite dependence of geophone orientation azimuth calculations on noise content, offset and depth. In reality, the effects of these three things are most likely related to each other. For example, a nearer source offset results in less energy from P-wave first arrivals being recorded on horizontal receiver components; this would skew the signal to noise ratio to be more heavily weighted towards noise, simply due to lower signal. Similarly, deeper receivers will generally have lower signal content due to effects such as geometrical spreading and Q-related attenuation. Studies such as Gagliardi and Lawton (2010) show that field data have these same relationships to noise, offset and depth though it is harder to separate the effects in a real data example. It may be useful to quantify these effects, but there are still certain obstacles to achieving a complete understanding; future work is needed in this regard.

The comparisons between the analytic (DiSiena) and inversion (Ferguson) methods showed potential strengths and weaknesses of each method. The inversion method seems to be superior when there is high noise content, but when the noise is weaker the analytic method seems to be stronger. Interestingly, effects of geophone depth are much less prominent in the inversion method. Examining the trends of the inversion results (Figures 17 - 20) suggests that this method is much more sensitive to source-receiver offset than it is to noise content; perhaps this is related to a need for a stability factor, but further testing is needed to understand this effect.

## CONCLUSIONS

- The calculation of geophone orientation azimuths is dependent on signal to noise ratio, source-receiver offset and receiver depth.
- Using the analytic (DiSiena) method, a signal to noise ratio of 1-2 seems to be the minimum required for statistically reliable azimuth calculations; these calculations generally produced a mean within 0.5° of the receiver's true orientation.
- Even using noise-free data, the analytic method produces standard deviations in orientation azimuth of about 0.11°.
- Larger source-receiver offsets produce more accurate azimuth calculations using both methods used in this study.
- Deeper receivers result in less accurate azimuth calculations for the analytic (DiSiena) method, but seem to have little effect on calculations using the inversion (Ferguson) method.
- The above parameters are difficult to separate since they are related to each other; however, deeper investigation might have some success in quantifying their effects.

## FUTURE WORK

A full statistical analysis of the inversion method is needed in order to fully understand its strengths and weaknesses. Additionally, tests of this method on real data should be performed, and the data window used should be examined. For both methods, it would be useful to develop some sort of quantitative relation of the effects of noise, offset and depth with orientation angle accuracy and precision. Finally, the relationship of the x-component noise and y-component noise should be considered more carefully, through both theory and field data.

## ACKNOWLEDGEMENTS

We would like to thank Rob Ferguson for providing us with the code necessary to implement his inversion method, and Heather Lloyd and Kevin Hall for their immense help in using TIGER. Finally, we would like to thank CREWES Sponsors.

## REFERENCES

DiSiena, J. P., Gaiser, J. E. and Corrigan, D., 1984, Three-component vertical seismic profiles; orientation of horizontal components for shear wave analysis, in Toksoz, M. N. and Stewart, R. R., eds., Vertical seismic profiling, Part B Advanced concepts: , 189-204.

Ferguson, R. J., 2009, Geophone rotation analysis by polarity inversion: CREWES Research Report, **21,** 20.1-20.12.

Gagliardi, P. and Lawton, D. C., 2010, Borehole geophone repeatability experiment: CREWES Research Report, **22,** 22.1-22.23.

Hokstad, K., Maaø, F., Nguyen, A. K. and Streich, R., 2009, 3D Anisotropic Elastic Finite-Difference Modeling in Transversely Isotropic Media: 1-45.